Self-organized biotectonics of termite nests

Alexander Heyde, Lijie Guo, Christian Jost, Guy Theraulaz, L. Mahadevan

Self-organized biotectonics of termite nests

Alexander Heyde, Lijie Guo, Christian Jost, Guy Theraulaz, L. Mahadevan

Self-organized biotectonics of termite nests

Alexander Heyde[a], Lijie Guo[b], Christian Jost[b], Guy Theraulaz[b], and L. Mahadevan[a,c,d,e,1]

[a]Department of Organismic & Evolutionary Biology, Harvard University, Cambridge, MA 02138; [b]Centre de Recherches sur la Cognition Animale (CRCA), Centre de Biologie Intégrative (CBI), Université de Toulouse, CNRS, UPS, Toulouse, France; [c]Paulson School of Engineering and Applied Sciences, Harvard University, Cambridge, MA 02138; [d]Department of Physics, Harvard University, Cambridge, MA 02138; [e]Kavli Institute for Bionano Science and Technology, Cambridge, MA 02138

This manuscript was compiled on April 16, 2020

The termite nest is one of the architectural wonders of the living world, built by the collective action of workers in a colony. Each nest has several characteristic structural motifs that allows for efficient ventilation, cooling, and traversal. We use tomography to quantify the nest architecture of the African termite *Apicotermes lamani*, consisting of regularly spaced floors connected by scattered linear and helicoidal ramps. To understand how these elaborate structures are built and arranged, we formulate a minimal model for the spatiotemporal evolution of three hydrodynamic fields—mud, termites, and pheromones—linking environmental physics to collective building behavior using simple local rules based on experimental observations. We find that floors and ramps emerge as solutions of the governing equations, with statistics consistent with our observations of *A. lamani* nests. Our study demonstrates how a local self-reinforcing biotectonic scheme is capable of generating a architecture that is simultaneously adaptable and functional, as well as relevant for a range of other animal-built structures.

collective animal behavior | termite nests | stigmergy | partial differential equations | morphogenesis

Termite nests are among the most complex and impressive structures produced by animal societies (1–3) and serve to create a microniche that allows for the controllable exchange of matter and energy with the environment (4–6). Even when compared with the many animal species that exhibit collective behaviors, including coordinated motion, active synchronization, or shared decision making (7, 8), the collective activities of social insects such as the highly eusocial termite are exceptional, in that they often lead to the formation of intricate physical structures: shelters (9), trail networks (10), and, most prominently, nests (1, 2). These structures are not merely the byproduct of animal behavior, however, since they also play a central role in regulating the flow of information necessary for their own construction and function. Nest building in social insects is thus considered an exemplar of functional self-organization, and studying this process can inform us about how structure and function emerge on multiple length and time scales in ecophysiology (11).

The eusocial termites of the genus *Apicotermes* typify the architectural complexity that can be produced by social insects. These termites, native to the savannahs and forests of Africa, construct small ovoid nests just 20–40 cm in diameter, located 5–50 cm underground (12). The nest structure must be efficiently constructed so as to be capable of passive ventilation and cooling (4–6, 13–15), while remaining habitable and traversable by the termites within. This is no small feat—given the scale and complexity of *Apicotermes* nests, it is not feasible that any single termite has a sufficiently broad cognitive map of the organization of the whole structure to coordinate the actions of the colony (16). Yet even in the absence of centralized control, these nests clearly show coherent structure at a global scale, pointing to the collective self-organization of several thousand termites acting only on their local conditions to produce global order (3, 11, 16).

Rather than sharing information by direct communication (such as via antennal contact or visible gestures), it is instead likely that *Apicotermes* workers communicate indirectly by coupling their building actions with the deposition of a local stimulus (such as a secreted building pheromone) in nearby substrate (17). This principle of behavioral and physical coupling during collective construction has already been implicated in the morphogenesis of the large termite mound structures which enclose the nest. Over the long length and time scales of the overall mound structure, the small internal tunnels and chambers within the mound influence the porosity of the mound material (2, 15), mediate their ventilation (5, 6), and suffice to explain the coarse features of the mound, e.g. its shape, size, and temporal evolution (18). However, this leaves open the question of how the internal structural motifs are formed and maintained at shorter length scales in the mound microstructure. More specifically, the architectural complexity of *Apicotermes* nests begs two important questions: First, what are the structural motifs within the nest, and how are they arranged? And second, how are they formed via the dynamic feedback loop between individual behavior and emerging structure in the nest construction process?

Digitization and structure of *Apicotermes* nests

To answer these questions, we first collected, scanned, and statistically analyzed nests of the species *Apicotermes lamani*.

Significance Statement

Termite nests are a remarkable example of functional self-organization that show how structure and function emerge on multiple length and time scales in ecophysiology. To understand the process by which this arises, we document the labyrinthine architecture within the subterranean nests of the African termite *Apicotermes lamani* and develop a simple mathematical model that relies on the physical and biological interactions between mud, termites, and pheromones in the nest. Our model explains the emergent formation of parallel floors connected by linear and helical ramps, consistent with observations of real nests. Overall the study of how physics and behavior couple together in architecture might serve as inspiration for the design and construction of sustainable human architectures.

Author contributions: A.H., G.T, and L.M. conceived of the study. C.J. collected and imaged nests. L.G. analyzed nest statistics. A.H. and L.M. formulated the mathematical model. A.H. performed the simulations and parameter sweeps. A.H., L.G., C.J., G.T, and L.M. discussed results and data, and A.H. and L.M. wrote the manuscript with input from all authors.

The authors declare no conflict of interest.

[1]To whom correspondence should be addressed. E-mail: lmahadev@g.harvard.edu

Two nests (MeMo14, Fig. 1A, and MeMo13, Fig. 1B) were collected near Libreville, Gabon (fig. S1), although one of these (MeMo13) showed too much internal damage for a statistical analysis. A third nest (MeMo80, Fig. 1C) was collected in 2008 near Pointe Noire in the Republic of the Congo (fig. S1); in this nest, we measured that workers had length 4-5 mm and height 2-3 mm, while soldiers had length 8-10 mm with a height of 2-3 mm. We digitized and imaged the excavated nests with a medical X-ray computed tomography (CT) scanner (Materials and Methods), allowing for non-destructive exploration of the complete three-dimensional structure of each nest.

All of the nests showed a similar external appearance, and based on our X-ray CT scans, also shared a similar internal architecture consisting of many floor layers arranged in parallel, with several vertical or diagonal pillars connecting adjacent floors (Fig. 1A-B). We recorded a video fly-through of these complex, 3D internal structures (Movie S1). To investigate these structures that enable termites to efficiently traverse their nests, we systematically searched the digitized *A. lamani* nests for open corridors connecting adjacent floors (Materials and Methods), and we identified several occurrences of two types of ramps (Fig. 1C): linear ramps in which an excavated path connects several floors along a linear incline, and helicoidal ramps, in which the path spirals around a central pillar while connecting adjacent floors. Helicoidal ramps in the nest had no preferred chirality, although a pair of co-occurring left-handed and right-handed helicoidal ramps was identified.

We then examined the internal architecture of two *A. lamani* nests (MeMo80 and MeMo14, see also Table S1) in order to quantify the spacing and arrangement of floors and ramps. For each nest, we assembled a series of 359 and 177 vertical slices respectively (Fig. 2A) and measured the thickness of each floor and the vertical spacing between floors (Fig. 2B). The floor thickness was on average 1.7 mm (median = 1.6 mm) in nest MeMo80, and on average 1.8 mm (median = 1.2 mm) in nest MeMo14. The floor spacing was on average 4.6 mm (median = 4.7 mm) in nest MeMo80, and on average 7.2 mm (median = 7.7 mm) in nest MeMo14. For both nests, the distribution of floor thickness had low variance (coefficient of variation (CV) = 0.31 in MeMo80, CV = 0.59 in MeMo14), and the distribution of floor spacing was similarly narrow (CV = 0.19 in MeMo80, CV = 0.22 in MeMo14), demonstrating that the flooring of the termite nests are arranged at regular vertical frequencies, with a strong continuity between adjacent floors (Fig. S1B-C).

Given this consistent arrangement of floors, we next investigated the positioning of ramps within the nests by measuring the horizontal distance from each ramp to the nearest ramp on the same floor (Fig. 2C). In MeMo80, we found a mean same-floor distance of 27.4 mm (median = 25.4 mm, CV = 0.41), and in MeMo14 this mean distance was 25.7 mm (median = 27.1 mm, CV = 0.33). We compared these measurements with the horizontal distance between ramps on adjacent floors. Because these ramps were often directly connected, this distance was much smaller for both nests, with a mean of 12.9 mm (median = 9.2 mm, CV = 0.79) in MeMo80, and a mean of 7.1 mm (median = 6.5 mm, CV = 0.47) in MeMo14. Hence, while ramps tended to be spaced at fairly large, regular intervals across a floor, they tended to be positioned near to ramps on adjacent floors, allowing for efficient vertical traversal between nest levels.

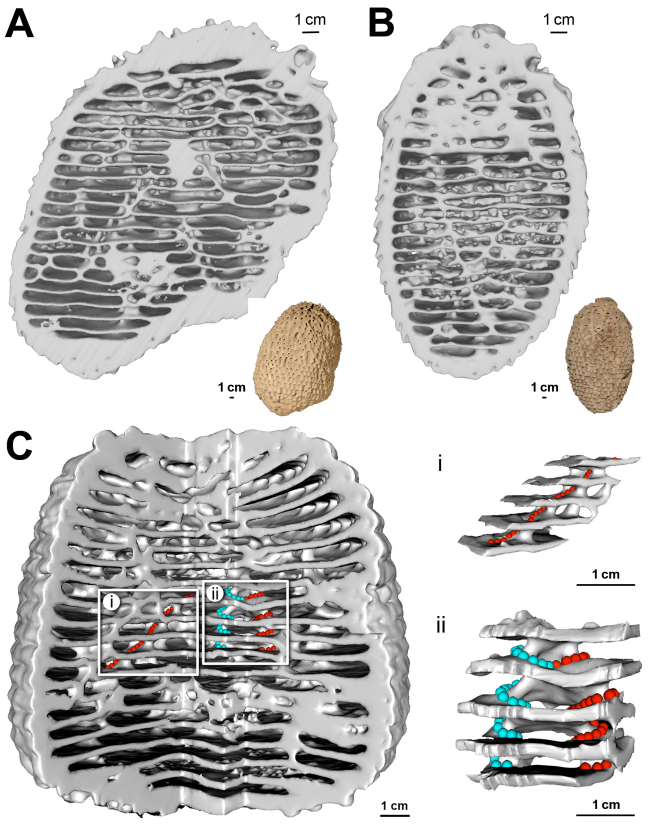

Fig. 1. Digital reconstruction of *Apicotermes lamani* nests reveals layered floors and chambers connected by linear and helicoidal ramps. (**A-B**) Cutaway view of two *A. lamani* nests, collected around Libreville (Gabon): MeMo14 (**A**) and MeMo13 (**B**). The nests were digitized with X-ray computer tomography and reconstructed in 3D. (**C**) A large *A. lamani* nest (left, MeMo80) collected in 2008 near Pointe Noire (Republic of the Congo) with examples of a linear ramp (i, red dots) and two helicoidal ramps with opposing chirality (ii, red and cyan dots).

A minimal model of termite tectonics

To address how these structures are formed, we turn to a series of observations, old and new, to motivate a minimal continuum theory of nest construction. With no evidence of design or a designer, termites build in response to local cues such as the nearby mound structure and secreted pheromones (17, 19). The resulting architecture both enables and constrains the movement of pheromones and termites, and thereby modifies behavior, so that nest construction can be seen as a result of a feedback loop linking physical and behavioral dynamics (Fig. 3A), similar to a recent model for the macrostructural morphogenesis of the termite mound (18). The architecture of the nest dictates which spaces are accessible to termite workers, the density of termite workers in turn controls the concentration of secreted pheromone, and the information carried by the pheromone profile in turn serves as a template for the ongoing remodeling of the nest architecture, thereby completing the feedback loop of nest morphogenesis.

We therefore model the spatiotemporal dynamics of three fields that depend on location denoted by the vector $\mathbf{x}$ and time t: the nest material density $u(\mathbf{x}, t)$, the termite worker density $n(\mathbf{x}, t)$, and the pheromone concentration $\rho(\mathbf{x}, t)$. These three fields jointly evolve according to a set of conservation laws, expressed as the following partial differential equations for the

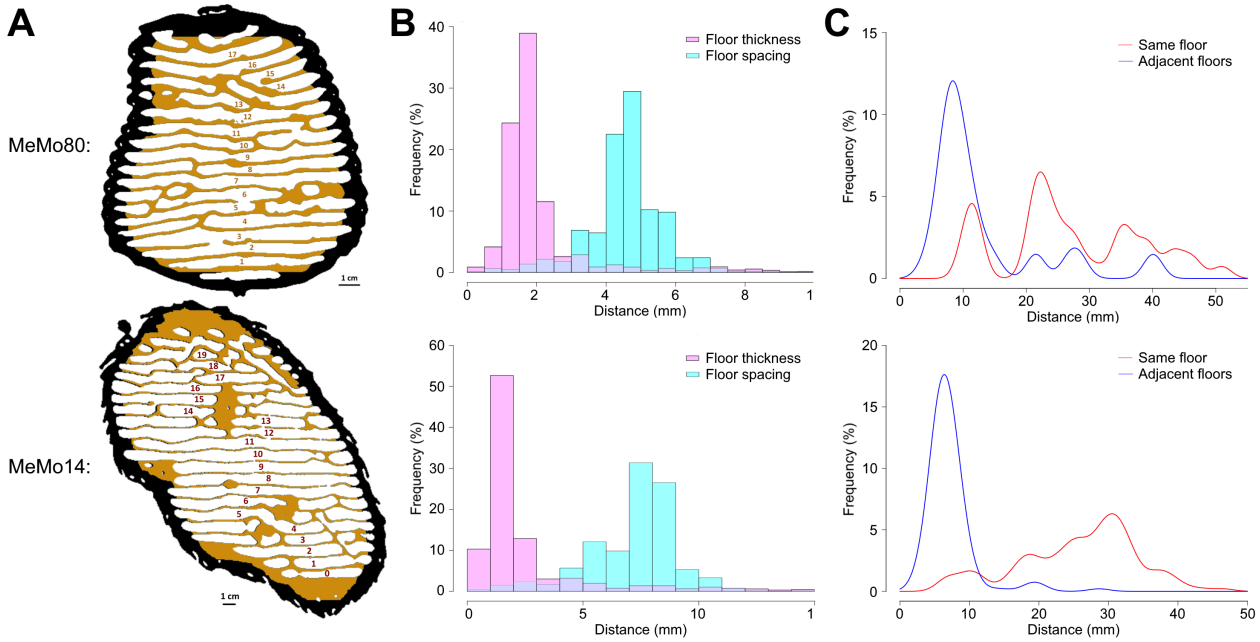

Fig. 2. Statistical analysis of *A. lamani* nests shows consistent floor and ramp spacing. Top row = nest MeMo80, bottom row = nest MeMo14. (**A**) Representative vertical slices of nest structure with floors labeled in average height order. (**B**) Histograms for floor thickness (pink) and spacing between floors (cyan), as measured in mm, corresponding to the nest depicted at left. Both the thickness of and spacing between floors tend to fall within a consistent band in each nest. (**C**) Density plot for the horizontal distance from a ramp to the nearest other ramp on the same floor (red) or on an adjacent floor above or below (blue), corresponding to the nest depicted at left. Ramps on the same floor tend to be spaced out, while ramps on adjacent floors often connect directly, resulting in minimal spacing.

nest material, termite workers, and pheromone levels:

$$\text{Nest material:}\quad \partial_t u = \partial_z \cdot [g\partial_z u] + f_+ - f_-, \qquad [1]$$

$$\text{Termite workers:}\quad \partial_t n_\pm = \nabla \cdot [(1-u)D\nabla n_\pm + \chi n_\pm \nabla u] \pm (f_- - f_+)k^{-1}, \qquad [2]$$

$$\text{Pheromone:}\quad \partial_t \rho = \nabla \cdot [\delta \nabla \rho] + H f_+ - \gamma\rho, \qquad [3]$$

where ∂_t and ∂_z are the differential operator in time and height respectively, $\nabla\cdot$ is the three-dimensional divergence operator, and ∇ is the three-dimensional gradient operator. Here Eq. 1 reflects the addition and removal of the nest material, with f_+ and f_- denoting the building and removal rates of dirt (whose functional form is discussed below). Moreover, the poroelastic diffusivity of dirt g captures its capacity to settle under the influence of gravity (20); this term breaks the rotational symmetry of the model equations and establishes a defined vertical orientation for the mound. Eq. 2 reflects the dynamics of termites carrying dirt n_+ or not carrying dirt n_-, with a flux that has two components: an effective diffusivity that is proportional to the amount of open space, i.e. $(1-u)D$, as well as a chemotactic term that drives termite workers into open and low-density nest regions with chemotactic coefficient χ. The final term represents switching between n_+ and n_-, with the pellet size k denoting the average amount of dirt transported by a termite worker. Lastly, Eq. 3 reflects the dynamics of secreted pheromones, driven by diffusion with a diffusion coefficient δ, production by termites at a rate H, and degradation at a rate γ. We note that the pheromone is relatively non-volatile and thus not advected by the ambient fluid, since the subterranean nests of *Apicotermes* do not typically have noticeable temperature gradients (21).

To complete the formulation of our model, we require functional forms for the building rate f_+ and removal rate f_-. Although these rates have not been directly measured in *A. lamani* termites, the building rate has been investigated for the neotropical termite *Procornitermes araujoi* (22), and both rates have also been quantified in the ant *Lasius niger* (23). In all cases we find that the local nest density scales directly with the building rate and inversely with the removal rate, resulting in high-density regions becoming increasingly compacted while low-density regions are excavated. Moreover the amplification of building rate scales with a pheromone added by the workers to the building material (Fig. 3B), so that the termites are more likely to deposit dirt in regions marked by pheromone as being sites of active remodeling, and so that building does not take place either where there is no nest material ($u = 0$) or where the nest material is already fully compacted ($u = 1$). It is reasonable also that the removal rate scales with the density of termite workers not carrying dirt and with the density of dirt u available for removal. Given these basic considerations, the simplest possible functional forms for f_+ and f_- are

$$\text{Building rate:}\quad f_+ = r_+ n_+ \rho u(1-u), \qquad [4]$$

$$\text{Removal rate:}\quad f_- = r_- n_- u, \qquad [5]$$

where $r_\pm$ are rate constants. With these choices, the dynamics of nest morphogenesis as described by our model can be captured by only a small number of non-dimensional parameters: the scaled pheromone potency Hr_+/r_-, the scaled evaporative flux γ/r_-, the pellet size k, and the scaled diffusivities δ/D, χ/D, and g/D (Materials and Methods). For simplicity, and to study the self-contained organization of this system, we model the nest as a closed three-dimensional domain, using no-flux boundary conditions, such that when integrated over the nest domain the total number of termites $|n|$ and the total quantity of dirt u are conserved.

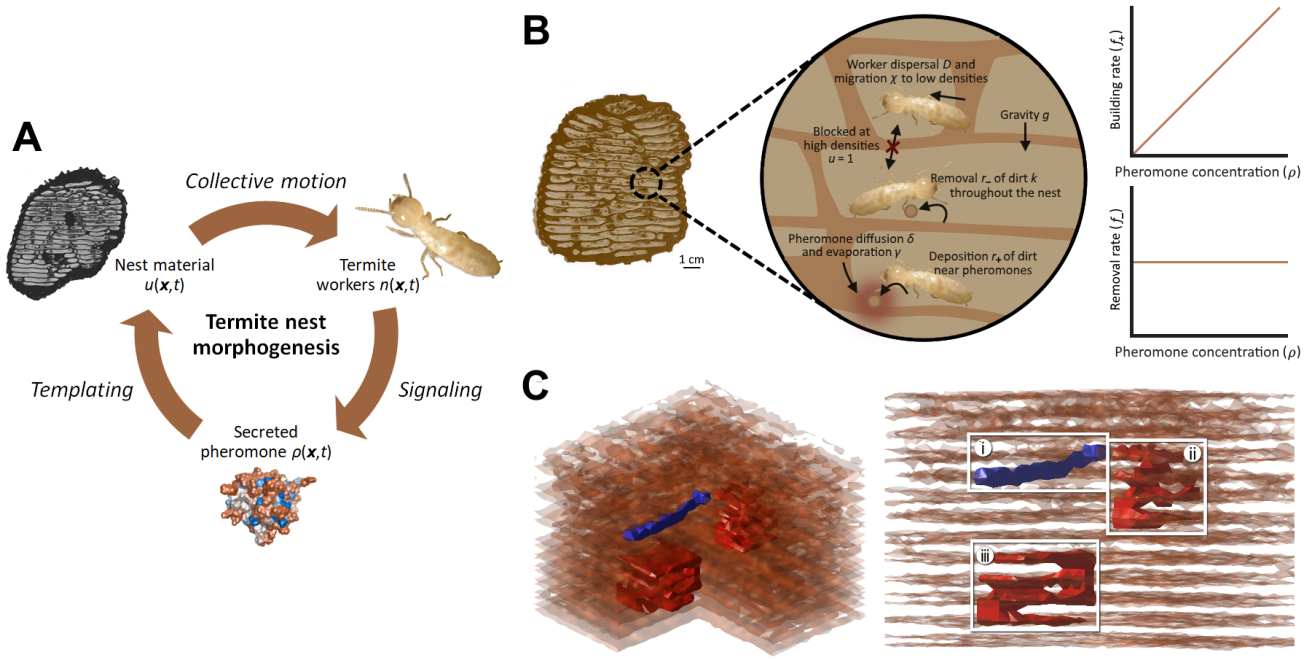

Fig. 3. Biotectonic model predicts floor spacing and ramp emergence in termite nests. (**A**) Model schematic of the feedback loop driving nest construction, highlighting the interactions between nest material u, termite workers n, and secreted pheromone ρ. (**B**) Illustration of a local region of a nest, showing the processes in our model. Termite workers migrate preferentially to low-density regions and cannot travel through very high-density regions. Workers remove dirt throughout the nest but are more likely to deposit dirt near pheromones which they release during deposition. Pheromones are assumed to have a low diffusivity and hence provide a local signal. (**C**) 3D reconstruction of a nest simulated according to our construction model, shown here at two angles. This simulated nest contains one linear ramp (i, blue) and two helicoidal ramps (ii-iii, red).

Natural patterns in simulated mounds

We conducted 500 independent simulations of nest construction by initializing our model each time with uniform nest density $u(\mathbf{x}, t)$ and pheromone concentration $\rho(\mathbf{x}, t)$, and with a uniform density of termite workers $n(\mathbf{x}, t)$, using measured and inferred parameter values from several studies on termite nest structure and behavior (Table S2) and a numerical implementation of an Euler differencing scheme (Materials and Methods). The model generated simulated nests (Fig. S2A-C) containing regularly spaced floors, with a mean planar orientation orthogonal to the direction of gravity and a floor thickness that scales as $(\delta/\gamma)^{1/2}$ in some regimes (Materials and Methods, Fig. S2D), which gives an average prediction of ∼1.9 mm, directly in line with our observed measurements of 1.7 mm and 1.8 mm in MeMo80 and MeMo14, respectively. Moreover, the simulated nests contained surface edges (topological defects) spanning across floors and sometimes forming traversable connections (Fig. 3C) corresponding to linear ramps (edge dislocations)—in which one floor terminates to provide the vertical space necessary for a simple ramp between adjacent floors—and helicoidal ramps (screw dislocations), which wind about a vertical pillar serving as a dislocation line spanning multiple floors (24) (Fig. S3).

By identifying the eventual location of a ramp, we observe the dynamical process by which ramps emerge from these defects during the construction process (Fig. 4A, Movie S2). Varying our model parameters by an order of magnitude on either side of our estimates, we find that only two parameters control whether helicoidal ramps form: the scaled pheromone potency Hr_+/r_- and the scaled pheromone evaporation rate γ/r_-, yielding a phase space for their emergence (Fig. 4B). This is consistent with previous agent-based simulations of ant nest construction that pointed to the central role of the pheromone evaporation rate in influencing nest structures (23).

A fly-through of our simulated nests (Movie S3) reveals the structural similarity of the simulated nests produced by our model with the scanned *A. lamani* nests. To quantitatively compare the simulated and scanned nests, we gathered an identical set of statistics to describe the simulated nest topologies. We found that the floor thickness and spacing between floors were similarly consistent in both the simulated and scanned nests, indicated by distributions with a similarly narrow variance (Fig. 4C). Moreover, the horizontal spacing between neighboring ramps on the same floor was substantially greater than the horizontal spacing between ramps on adjacent floors that often connected directly, as observed in the scanned nests (Fig. 4D). To assess the similarity of the simulated and scanned nests on large scales, we carried out a spectral analysis of the average nest density as a function of height for both the scanned and simulated nests and found that these density profiles are very similar (Fig. 4E). Together, these metrics indicate that the simulated nests resemble natural nests across global and local scales.

Emergent biotectonics from physics and behavior

Our minimal theoretical framework links three spatiotemporal fields involved in the biotectonics of termite nests: dirt to constitute the nest, termite workers to shape the nest, and secreted pheromone to mark active regions of the nest. They allow us to capture two key geometrical and topological features of termite nests, namely the regular vertical spacing of floors and the horizontal spacing of ramps on the same or adjacent

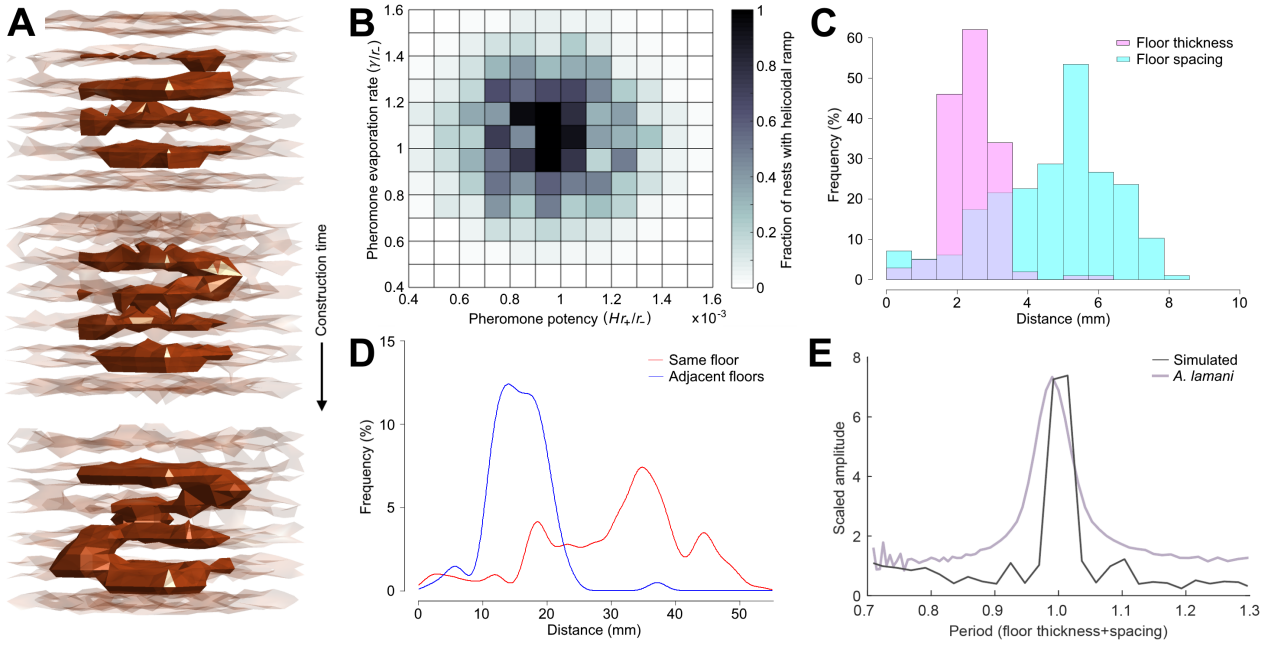

Fig. 4. Simulated nests resemble natural *A. lamani* nests and produce helicoidal ramps across a range of parameters. (**A**) Time snapshots of helicoidal ramp emergence during simulated nest construction, from early (top) to late (bottom) in the building period. (**B**) Heatplot for the frequency of helicoidal ramps in a simulated nest as a function of the two model parameters governing pheromone dynamics. (**C**) Histograms for floor thickness (pink) and spacing between floors (cyan), as measured in mm, averaged over simulated nests. The histograms show a pattern similar to the natural nests in Fig. 2B. (**D**) Density plot for the horizontal distance from a ramp to the nearest other ramp on the same floor (red) or on an adjacent floor above or below (blue), averaged over simulated nests and resembling the natural patterns shown in Fig. 2C. (**E**) The power spectrum of nest density, averaged over horizontal slices, peaks sharply at a period of two floor heights for both simulated (gray) and natural (purple) nests, indicating regularly spaced floor structures.

floors. This feedback loop involving architecture, behavior, and information that drives nest construction is likely to be quite general; it is implicated also in the macromorphogenesis of termite mounds (18) and might additionally provide insight into emergence of other animal architectures, such as ant nests, beehives or other termite subfamilies (1, 23, 25, 26). The finding that the nest structure emerges spontaneously for a range of parameter values points to it being a nonequilibrium steady state that is robust and adaptable—a direct consequence of the ability of a colony to both lay down and respond to cues in its environment.

An important open question is the role of heat gradients and air flow within the nest (5, 6, 15), which are determined by the nest structure and in turn help to propagate pheromones and other signals, such as carbon dioxide levels (27). The pheromones we consider here have low diffusivities (19) so as to provide a localized signal useful in nest construction, such that heat-driven air flow results in a negligible change when incorporated into our model (SI Text, Fig. S4); however, other odors with a higher diffusivity, such as those secreted by the queen, would be more susceptible to internal nest flow, and hence more important to the larger-scale problem of the global templating and emergence of overall mound shape (18, 19). In the subterranean nests of *Apicotermes*, we expect that the role of heat gradients and air flow is minor relative to above-ground nests which are directly subjected to sunlight and air currents.

The spontaneous emergence of these functional, palatial architectures from the construction dynamics of social insects interacting with the environment stands in stark contrast to planned human architectures that break down on moderate to large scales. Perhaps by studying the natural structures that termites and other insects build and rely upon, and by understanding the coupling of physical and behavioral processes that underlie their morphogenesis, we can take inspiration for the design and construction of sustainable human architectures (28). After all, while we as humans have a mere ∼400,000 years of experience with constructing primitive structures (29), mound-building termites of the family Termitidae have spent close to 50 million years (30) developing one of the grandest examples of architecture in the natural world.

Materials and Methods

X-ray computed tomography (CT). Each nest was imaged using X-ray computed tomography with a medical scanner and reconstructed into a series of virtual cuts (512×512 pixels). MeMo13 and MeMo14 were scanned with a Somatom Sensation16 (Siemens, Erlangen, Germany) at CHU Toulouse Rangueil, France using exposure parameters of 120 kV and 150 mAs, slice thickness of 1 mm, interslice distance 0.5 mm. MeMo80 was scanned with a LightSpeed Ultra (GE Medical Systems, Buc, France) at CHU Dijon using exposure parameters 100 kV and 170 mAs, slice thickness of 0.625 mm, interslice distance 0.3 mm. Reconstruction of the virtual cuts (Fig. 1) was performed in the open-source software Horos (LGPL license).

Investigation of internal structures. Ramps (with connecting holes to the floor above) and pillars (supporting the above floor without a passway) were identified by visual inspection of three orthogonal planes at each voxel of the original CT in the Horos software. For helices, identification was confirmed by reconstructing a perspective view (3D Surface Rendering) that could be inspected from all sides (e.g. Fig. 1C). Mean coordinates for the base of each ramp or pillar were extracted (Fig. 2A) for the statistics in Fig. 2C and Table S1. For Fig. 2B, MeMo14 was rotated to align horizontal floors with the x-y plane (imageJ/Fiji, rotate tool with bilinear interpolation). Images were then binarized in imageJ with a threshold calibrated by visual comparison between the resulting structures, the original grey-scale tomograph images, and photos of cut-open same-species nests. The outer walls were removed by first dilating each slice five

times to close all outside openings, and then using the wand tool to define an outline ROI of the nest for each slice (also used to compute the total nest volume). All pixels outside the new ROIs were removed to obtain nests without outer walls as in Fig. 2A.

Floor thickness and floor spacing were measured by counting the number of consecutive black or white pixels in each vertical pixel line of the stacked images, with code written in R. The presence of pillars/ramps led to heavy right tails in both distributions, which were removed by cutting off all measures above twice the median floor height and alpha-trimming the resulting distributions with $\alpha = 0.02$ on both sides. To check for the continuation of ramps across several floors, we selected for each floor the horizontal slice for which the horizontal pixel density was minimal (Fig. S1B), computed the correlation coefficient between the pixels of adjacent floors, and compared them to the correlation coefficients between slices at least three floors separated (Fig. S1C).

Non-dimensionalization of construction model. Using the dimensional parameters given in Table S2, we can construct five non-dimensional parameters that allows us to rewrite Eqs. 1-5 in terms of a series of normalized variables $T = r_- t$, $\mathbf{X} = \mathbf{x}/\ell$, $\tilde{\nabla} = \ell\nabla$, and $P = \rho r_+/r_-$ for time, position, gradient, and pheromone concentration respectively, where $\ell = (r_-/D)^{1/2}$ denotes the length scale used here for normalization. This gives the non-dimensional system

$$\partial_T u = \partial_Z \cdot [\tfrac{g}{D}\partial_Z u] + f_+ - f_-, \quad [6]$$

$$\partial_T n_\pm = \tilde{\nabla} \cdot [(1-u)\tilde{\nabla} n_\pm + \tfrac{\chi}{D} n_\pm \tilde{\nabla} u] \pm (f_- - f_+)k^{-1}, \quad [7]$$

$$\partial_T P = \tilde{\nabla} \cdot [\tfrac{\delta}{D}\tilde{\nabla} P] + \tfrac{Hr_+}{r_-} f_+ - \tfrac{\gamma}{r_-} P, \quad [8]$$

with $f_+ = n_+ P u(1-u)$ and $f_- = n_- u$. These coupled equations contain a set of dimensionless parameters that are the scaled pheromone potency Hr_+/r_-, the scaled evaporative flux γ/r_-, the pellet size k, and the scaled diffusivities δ/D, χ/D, and g/D that control the range of possible outputs from our model.

Analysis of construction model. Our model permits the derivation of a simple scaling prediction regarding the regularity of floor thickness. At steady state, the building and removal rates must be balanced:

$$f_+ - f_- = r_+ n_+ \rho u(1-u) - r_- n_- u = 0. \quad [9]$$

In terms of the steady state ratio $\eta = n_-/n_+$ of termite workers without dirt, this balance leads to either a no-density tunnel or chamber ($u = 0$) or a high-density floor or wall with density value

$$u^* = 1 - \tfrac{\eta r_-}{\rho r_+}. \quad [10]$$

To understand which of these steady states is stable we need to evaluate the stability condition $\partial_u(f_+ - f_-) < 0$ (see SI). This reveals that the tunnels ($u = 0$) occur when the pheromone level is low ($\rho < \eta r_-/r_+$); since in these regions $f_+ = f_- = 0$, the pheromone profile converges to $\rho(x) = 0$. In contrast, structures ($u = u^*$) occur when the pheromone level is high ($\rho > \eta r_-/r_+$), and in the vicinity of a structure, building and removal are balanced at rate $f_+ = f_- = r_- n_+ \eta u^*$.

In the SI, we show that regularly spaced floors require that the condition $0 \leq \alpha \leq 1$ needs to be satisfied, where $\alpha = 1 - 4\gamma/Hr_+$. This allows us to derive an expression for the thickness L of a floor which follows the approximate scaling law

$$L \sim \left[\frac{\gamma}{\delta} - \frac{Hr_+}{4\delta}(1-\sqrt{\alpha})\right]^{-1/2}. \quad [11]$$

In the regime $\alpha \approx 1$, for example, the floor thickness scales as $L \sim \sqrt{\delta/\gamma}$, the prediction one would expect in the case where floors are fully packed, $u^* \approx 1$. This regime is characterized by slow pheromone evaporation relative to its high deposition rate and potency. For our parameter values, this thickness is a realistic 1.9 mm. For the alternative extremal case $\alpha \approx 0$, in which the pheromone evaporation is sufficiently high to result in more diffuse nest interiors, the scaling law depends also on H and r_+, as plotted in Fig. S2D, consistent with our full numerical simulations.

Numerical solution of model equations. To simulate our construction model, we implemented a finite difference solver to numerically integrate the system of equations [1-5]. We initialized each simulation with uniform nest density $u = 0.5$ (halfway packed) and uniform pheromone concentration $\rho = 0.1\,\mathrm{ng/cm^3}$, and with randomly scattered termite workers, such that the density of termites n at each grid location x was drawn from an exponential distribution with non-dimensional mean 0.1. At each time step, the gradient and Laplacian of each of the three fields was calculated using second-order differencing in space, and the nest interior was then updated with first-order differencing in time. For each set of model parameters, 500 independent simulations were conducted.

ACKNOWLEDGMENTS. We thank A. Robert for providing nest MeMo80 and the natural history museum in Paris for providing nests MeMo13 and MeMo14, both collected by Grassé. This work was supported by NSF Grant DGE-1144152 (to A.H.), ANR Grant ANR-06-BYOS-0008 (to G.T.), CSC PhD Grant (to L.G.), and the NSF Physics of Living Systems Grant PHY1606895 (to L.M.).

1. M Hansell. *Animal architecture*. Oxford University Press, 2005.
2. A Perna and G Theraulaz. When social behaviour is moulded in clay: on growth and form of social insect nests. *J. Exper. Biol.*, 220(1):83–91, 2017.
3. CC Lee, KB Neoh, and CY Lee. Caste composition and mound size of the subterranean termite macrotermes gilvus (isoptera: Termitidae: Macrotermitinae). *Annals Entomological Soc. Amer.*, 105(3):427–433, 2012.
4. JS Turner. On the mound of macrotermes michaelseni as an organ of respiratory gas exchange. *Physiological and Biochemical Zoology*, 74(6):798–822, 2001.
5. H King, SA Ocko, and L Mahadevan. Termite mounds harness diurnal temperature oscillations for ventilation. *Proc. Natl. Acad. Sci. U.S.A.*, 112(37):11589–11593, 2015.
6. SA Ocko, H King, D Andreen, P Bardunias, JS Turner, R Soar, and L Mahadevan. Solar-powered ventilation of african termite mounds. *J Exper. Biol.*, 220(18):3260–3269, 2017.
7. S Camazine, JL Deneubourg, NR Franks, J Sneyd, E Bonabeau, and G Theraulaz. *Self-organization in biological systems*, volume 7. Princeton University Press, 2003.
8. DJT Sumpter. *Collective animal behavior*. Princeton University Press, 2010.
9. C Anderson and DW McShea. Intermediate-level parts in insect societies: adaptive structures that ants build away from the nest. *Insectes Sociaux*, 48(4):291–301, 2001.
10. TJ Czaczkes, C Grüter, and FLW Ratnieks. Trail pheromones: an integrative view of their role in social insect colony organization. *Ann. Rev. Entomology*, 60:581–599, 2015.
11. E Bonabeau, G Theraulaz, JL Deneubourg, S Aron, and S Camazine. Self-organization in social insects. *Trends Ecol. & Evol.*, 12(5):188–193, 1997.
12. J Desneux and AE Emerson. Les constructions hypogées des apicotermes termites de l'afrique tropicale. *Annales du Musée Royale du Congo Belge, Sciences Zoologiques*, 17, 1952.
13. RS Schmidt. Functions of apicotermes nests. *Insectes Sociaux*, 7(4):357–368, 1960.
14. J Korb and KE Linsenmair. The architecture of termite mounds: a result of a trade-off between thermoregulation and gas exchange? *Behav. Ecol.*, 10(3):312–316, 1999.
15. K Singh, BP Muljadi, AQ Raeini, C Jost, V Vandeginste, MJ Blunt, G Theraulaz, and P Degond. The architectural design of smart ventilation and drainage systems in termite nests. *Sci. Advances*, 5(3):eaat8520, 2019.
16. G Theraulaz and E Bonabeau. A brief history of stigmergy. *Artificial Life*, 5(2):97–116, 1999.
17. PP Grassé. La reconstruction du nid et les coordinations interindividuelles chezbellicositermes natalensis etcubitermes sp. la théorie de la stigmergie: Essai d'interprétation du comportement des termites constructeurs. *Insectes Sociaux*, 6(1):41–80, 1959.
18. SA Ocko, A Heyde, and L Mahadevan. Morphogenesis of termite mounds. *Proc. Natl. Acad. Sci. U.S.A.*, 116(9):3379–3384, 2019.
19. OH Bruinsma. *An analysis of building behaviour of the termite Macrotermes subhyalinus (Rambur)*. PhD thesis, Bruinsma, 1979.
20. JM Skotheim and L Mahadevan. Dynamics of poroelastic filaments. *Proc. Roy. Soc. London. A*, 460(2047):1995–2020, 2004.
21. RS Schmidt. Apticotermes nests. *Amer. Zoologist*, pages 221–225, 1964.
22. D Fouquet, AM Costa-Leonardo, R Fournier, S Blanco, and C Jost. Coordination of construction behavior in the termite procornitermes araujoi: structure is a stronger stimulus than volatile marking. *Insectes Sociaux*, 61(3):253–264, 2014.
23. A Khuong, J Gautrais, A Perna, C Sbaï, M Combe, P Kuntz, C Jost, and G Theraulaz. Stigmergic construction and topochemical information shape ant nest architecture. *Proc. Natl. Acad. Sci. U.S.A.*, 113(5):1303–1308, 2016.
24. JP Hirth, J Lothe, and T Mura. Theory of dislocations, 1983.
25. V Škarka, JL Deneubourg, and MR Belić. Mathematical model of building behavior of apis mellifera. *J Theor. Biol.*, 147(1):1–16, 1990.
26. A Perna, S Valverde, J Gautrais, C Jost, R Solé, P Kuntz, and G Theraulaz. Topological efficiency in three-dimensional gallery networks of termite nests. *Physica A: Stat. Mech. and its Applications*, 387(24):6235–6244, 2008.
27. MD Cox and GB Blanchard. Gaseous templates in ant nests. *J Theor. Biol.*, 204(2):223–238, 2000.
28. JS Turner and RC Soar. Beyond biomimicry: What termites can tell us about realizing the living building. In *First International Conference on Industrialized, Intelligent Construction at Loughborough University*, 2008.
29. P Villa. Terra amata and the middle pleistocene archaeological record of southern france. *University of California Publications in Anthropology Berkeley, Cal*, 13, 1983.
30. DA Arab, A Namyatova, TA Evans, SL Cameron, DK Yeates, SYW Ho, and N Lo. Parallel evolution of mound-building and grass-feeding in australian nasute termites. *Biol. Letters*, 13 (2):20160665, 2017.